



THE UNIVERSITY *of* EDINBURGH

## Edinburgh Research Explorer

### Vortices, dissipation and flow transition in volatile binary drops

**Citation for published version:**

Bennacer, R & Sefiane, K 2014, 'Vortices, dissipation and flow transition in volatile binary drops', *Journal of Fluid Mechanics*, vol. 749, pp. 649-665. <https://doi.org/10.1017/jfm.2014.220>

**Digital Object Identifier (DOI):**

[10.1017/jfm.2014.220](https://doi.org/10.1017/jfm.2014.220)

**Link:**

[Link to publication record in Edinburgh Research Explorer](#)

**Document Version:**

Peer reviewed version

**Published In:**

Journal of Fluid Mechanics

**General rights**

Copyright for the publications made accessible via the Edinburgh Research Explorer is retained by the author(s) and / or other copyright owners and it is a condition of accessing these publications that users recognise and abide by the legal requirements associated with these rights.

**Take down policy**

The University of Edinburgh has made every reasonable effort to ensure that Edinburgh Research Explorer content complies with UK legislation. If you believe that the public display of this file breaches copyright please contact [openaccess@ed.ac.uk](mailto:openaccess@ed.ac.uk) providing details, and we will remove access to the work immediately and investigate your claim.



# Vortices, dissipation and flow transition in volatile binary drops

R. BENNACER<sup>1</sup> and K. SEFIANE<sup>2†</sup>

<sup>1</sup>LMT, Ecole Normale Supérieure Cachan, F-94235 Cachan, France

<sup>2</sup>School of Engineering, The University of Edinburgh, Edinburgh EH9 3JL, UK

(Received ?; revised ?; accepted ?. - To be entered by editorial office)

Despite its fundamental and practical relevance, flow structure and evolution within volatile mixture drops remains largely unexplored. We study experimentally, using particle image velocimetry (PIV), the evolution of internal flow during the evaporation of ethanol-water mixture drops for different initial concentrations. The investigation revealed the existence of three stages in the evolving flow behaviour within these binary volatile drops. We propose an analysis of the nature of the flow and focus on understanding successive flow stages as well as transition from multiple vortices to a monotonous outward flow. We show that the existence of multiple vortices during the first stage is driven by local concentration gradients along the interface. When the more volatile component (in this case ethanol) is depleted, the intensity of this *Marangoni* flow abruptly declines. Towards the end of the first stage, ethanol is driven from the bulk of the drop to the interface to sustain weakening concentration gradients. Once these gradients are too weak, the solutal *Marangoni* number becomes sub-critical and the driving force for the flow switches off. The evolution of flow structure and transition between stages is found to be well correlated with the ratio of Marangoni and Reynolds numbers. Furthermore, we argue that whilst the observed vortices are driven by surface tension shear stress originating at the liquid/vapour interface, the transition in flow and its dynamics is entirely determined by viscous dissipation. The comparison between the analytical expression for vorticity decay based on viscous dissipation and the experimental data show a very good agreement. The analysis also shows that regardless of the initial concentration, for same size drops, the transition in flow follows exactly the same trend. This further supports the hypothesis of a viscous dissipation transition of the flow. The last stage is satisfactorily explained based on non-uniform evaporation and continuity driven flow.

**Key words:** Drops, Evaporation, Marangoni flows, Wetting.

---

## 1. Introduction

Since the pioneering work of Young (1805), the interaction of liquid drops with solid substrates has been a subject of interest to scientists for more than a century. This phenomenon, known as wetting, is recognised as being crucial in a wide range of biological, natural and industrial processes. When drops are deposited on solids in unsaturated atmosphere, they evaporate at a rate which depends on relative saturation and ambient conditions. This process of evaporation and drying of sessile drops on solid substrates has attracted wide interest amongst researchers over the last decade, Deegan *et al.* (1997), Hu

† Email address for correspondence: ksefiane@ed.ac.uk

& Larson (2006), Sefiane *et al.* (2009), Erbil (2012). The evaporation of drops and their profile evolution and dependence on ambient conditions has been subject to numerous studies. Various aspects of this phenomenon have been experimentally and theoretically explored, including diffusion of vapour in the ambient medium, Sefiane *et al.* (2009) and substrate properties, Sefiane & Bennacer (2011). The dynamics of drop profile and three phase contact line and their dependence on substrate roughness and properties has also been extensively researched. Recent reviews on this topic could be consulted for a more detailed description of the phenomenon, Erbil (2012). Besides the evolution of drops profile and the kinetics of evaporation another aspect, equally important, has attracted the attention of researchers. This is the flow characteristics, nature and evolution within these volatile drops. In small enough evaporating drops, fluid flow can be driven either by continuity, Deegan *et al.* (1997), or surface tension gradients, Hu & Larson (2006), *i.e.* Marangoni. In the case of single component drops, the continuity flow is found to be mainly an outward flow driven by mass conservation, Deegan *et al.* (1997), Hamamoto *et al.* (2011). Another origin of the flow in volatile drops, is linked to *Marangoni* flow driven by surface tension gradients, Hu & Larson (2006). It is widely accepted that surface tension gradients along a liquid-vapour interface generate fluid flow known as Marangoni flow. The orientation and intensity of this flow in the case of single component drops can depend on the relative thermal properties of the substrate and liquid, Ristenpart *et al.* (2007). Furthermore, these flows can be the result of temperature and/or concentration gradients and may play a major role in energy transport, Ghasemi & Ward (2010). Generally, surface tension driven flows in single component volatile drops are essentially thermocapillary in nature, *i.e.* driven by temperature gradients.

In comparison with single component evaporating drops, the evaporation of binary and multicomponent drops in general, has received rather limited attention, Rowan *et al.* (2000), Sefiane *et al.* (2008). The few existing studies have focused essentially on studying the evolution of the drop profile of the mixture drop. Researchers agree on the observation that evaporation proceeds in distinct stages, a first stage where the more volatile component evaporates, a second stage which is a mixed stage and a last stage where the drop behaves as if it mainly consists of the less volatile component. These evaporation stages have been revealed through observations and measurements of the drop profile such as the angle, height, volume and base, Hopkins & Reid (2006), Cheng *et al.* (2006). It is worth stressing that during the evaporation of binary mixture drops, additional physical mechanisms, which are absent in single component drops contribute to the observed behaviour. Because of selective evaporation, the more volatile component evaporates first. This component has to diffuse from the bulk liquid of the drop to the interface. Once at the interface it evaporates and then diffuses in the gas phase, usually a mixture of vapour and air. The described process continues until the more volatile component is depleted and the remaining volume is essentially comprised of the less volatile one. Some traces of the volatile component could however persist till the end of the drop lifetime. As far as surface tension flows are concerned, the evaporation of binary mixture drops introduces a new effect which is not present in the case of single component drops. This effect is related to local concentration gradients on the interface and the resulting surface tension stresses and solutal Marangoni flows. Recently, a study used Particle Image Velocimetry (PIV) to characterise the flow within an evaporating binary mixture drop consisting of ethanol and water, Christy *et al.* (2011). This study revealed the existence of three stages in flow structure. The first stage corresponds to the existence of multiple convection vortices, the number of which reduces in time until the end of the first stage. This is followed by a second stage, the transition stage, which corresponds to a

transition of the flow structure from multiple vortices to an outward flow which is typical of pure water evaporating drops. The transition occurs very rapidly, in few seconds and the evolution of vorticity intensity in time exhibits an exponential decay. In an attempt to explain these observations it has been suggested that diffusion of the last content of ethanol in the liquid phase from the bulk to the interface could be the physical mechanism responsible for the transition in flow. Limited data however did not allow further exploration and quantification of the true mechanism(s) behind the observed transition in flow. It has been deduced, from this study, Christy *et al.* (2011), that the observed flow structure in the first stage is driven by surface tension gradients on the interface. These surface tension gradients are a direct result of concentration gradients. Indeed, concentration of ethanol (or water) on the interface affects the surface tension locally. The local concentration of ethanol on the interface is a result of the various processes taking place, namely diffusion in liquid from the bulk to the interface, evaporation, and diffusion into the gas phase. Since there is a limited reservoir of ethanol within the drop, concentration gradients on the interface tend to evolve with evaporation till total evaporation. **The study of Christy *et al.* (2011) was however limited to one single initial concentration namely 5 % of aqueous ethanol. Also the interpretation of the successive stages were not thoroughly examined.**

It is clear that a full understanding of the nature of internal flow within evaporating drops in general is far from being complete. Furthermore, the flow within binary volatile drops remains, to the best of our knowledge, largely unexplored. **Amongst the outstanding questions is the role played by the initial concentration in the observed stages of flow. Providing a physical interpretation for each of the observed stages of evaporating binary drops is also missing. This paper presents new data about internal flow structure and transition during the evaporation of binary mixture drops. Ethanol-water drops at various initial concentrations, evaporating under ambient conditions are investigated using particle image velocimetry technique to reveal the flow field and its evolution. The study shows that a first stage in the evaporation process is characterised by multiple vortices whose number decreases in time. The space-averaged intensity of vorticity remains however fairly constant during this first stage. The transition from multiple vortices to an outward monotonous flow occurs during a relatively rapid stage characterised by an exponential decline in vorticity. When normalised with the initial vorticity of the first stage, the transition stage is found to follow the same trend for all initial concentrations whose decay constant depends on drop size.**

The paper is organised as follows, in a first section (**Section 2.**) we present the experimental data on evaporation stages obtained from drop shape analysis and flow field obtained using Particle Image Velocimetry (PIV) for three initial concentrations and discuss observed trends. In the following section (**Section 3.**), we perform an analysis of the main physical mechanisms likely responsible for the observed flow. The first stage of evaporation is discussed in *sub-section 3.1*. In *sub-section 3.2*, we analyse the transition in flow and compare the analytical solution obtained from a viscous dissipation and decay of vorticity model with the experimental data. Finally in *sub-section 3.3*, we discuss the outward flow observed in the last stage of evaporation.

## 2. Experimental Results

The experimental set-up and procedures are similar as in Christy *et al.* (2011) and are briefly recalled hereafter. Ethanol-water mixture drops of  $0.12 \mu\text{l}$  ( $\pm 0.03 \mu\text{l}$ ) volume are

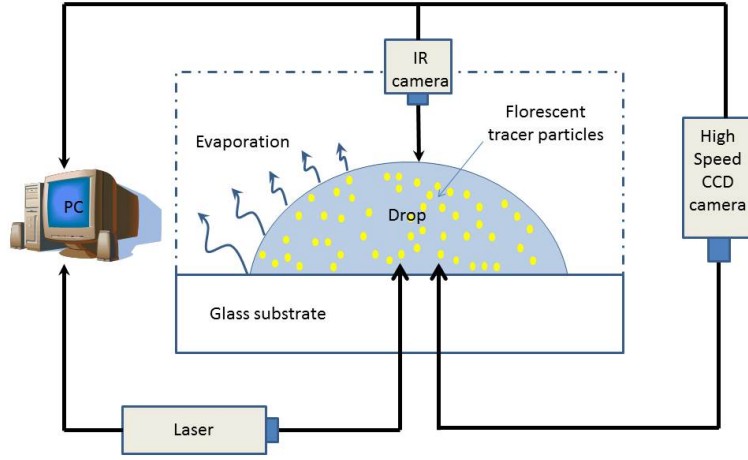


FIGURE 1. Schematic of the experimental setup.

seeded with 0.04 % tracers of fluorescent micro-spheres ( $1 \mu\text{m}$  diameter, Nilered, carboxylate modified FluoSphere<sup>®</sup> beads of density  $1.05\text{g}/\text{cm}^3$ ). The drops were deposited on a transparent glass substrate, sitting on an inverted microscope (Leica DM15000 M). The base radii of the sessile drops ranged from 0.9 mm to 1.1 mm, depending on ethanol concentration (0.9 mm for 5%, 1mm for 25% and 1.1 mm for 50%). A New Wave Pegasus pulse diode laser emitting at 527 nm, illuminated the drops from beneath causing the particles to fluoresce at 575 nm. A high speed camera, a Dantec Dynamics Nanosense II camera ( $512 \times 512$  pixels) is synchronized with the laser and captured the experiment at 20/100 Hz with a spatial resolution of 320 pixels/mm. The above PIV technique is used to map the flow in ethanol-water mixture drops evaporating at ambient conditions. Imaging the drop from beneath revealed flow maps as cross sections adjacent to the base of the drop, Figure 1 and Figure 4. The measured vorticity is a 2D section and represents the intensity and structure of the flow in the drop. Profiles of flow velocity along the base radius of the drop are extracted and plotted versus time. Three initial ethanol in water concentrations were studied, 5%, 25% and 50%, per volume. For the two higher concentrations of 25% and 50%, a higher data acquisition frequency of 100 Hz is used instead of 20 Hz used in the case of 5%. The reason for using higher acquisition frequency for high concentrations is the shorter lifetime and higher flow velocity. Typical measured flow velocities during the first stage are of the following magnitude,  $10^{-6}\text{m}/\text{s}$ ,  $10^{-5}\text{m}/\text{s}$  and  $10^{-4}\text{m}/\text{s}$  for 5%, 25% and 50% respectively.

### 2.1. Evaporation stages

In addition to PIV flow measurements, a Drop Shape Analysis instrument DSA100 from Kruss GmbH was simultaneously used to measure volume and base diameter evolution in time. The evaporation rate as a function of time is thus deduced and plotted in Figure 2. The data for evaporation rate indicate that during the first stage, stage I, the evaporation rate decreases for all concentrations studied. This is in contrast with the evaporation of a pure, pinned water drop, where evaporation rate remains fairly constant. The decline in evaporation rate can be understood in terms of reduction of ethanol content. As shown by the vapour pressure equilibrium phase diagram, in Figure 3 (inset), as ethanol

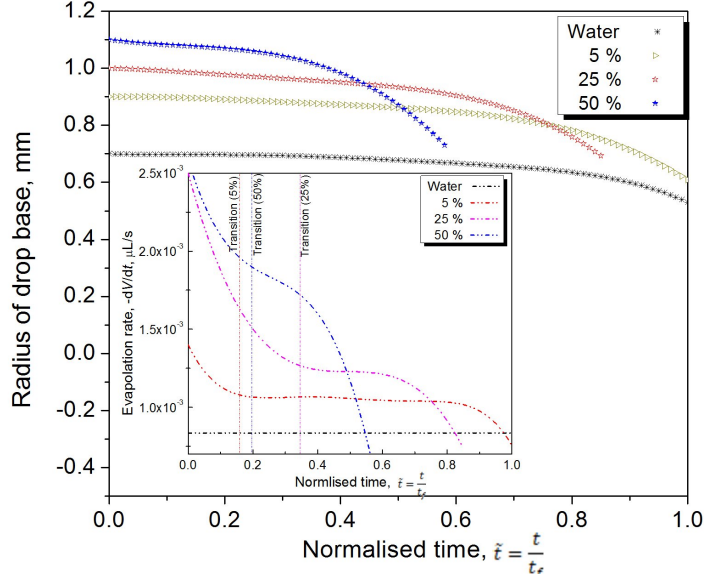


FIGURE 2. Drop radius evolution and evaporation rate (inset) in time for the three studied compositions and pure water for reference. The transition from stage (I) to Stage (II) is highlighted. The transition *i.e.* stage II, being very rapid, the first and last stages are the most noticeable.

concentration decreases, the vapour pressure decreases, hence evaporation. At the end of this decline in evaporation rate, transition in flow structure occurs. The transition is rapid and is followed by a constant evaporation rate similar to pure water during most of the last stage, stage III. The evaporation rate for a pure water drop is given in Figure 2 as a reference. Evaporation rates tend to consistently increase with increasing ethanol initial concentration. On the other hand the lifetime of the drops decreases with increasing ethanol concentration. The data for the base radius show that overall, the contact line remains pinned and sharply decreases towards the end of the drop lifetime, Figure 2. This is due to the presence of tracer particles which tend to self-pin the contact line. The last stage in evaporation of mixture drops exhibits a plateau in the overall evaporation rate which is greater than pure water case, this is probably due to the differences in drops base radii and to possible traces of ethanol left within the drop. Worth noting that the transition in stage II, occurs over a very short time, less than few seconds. It is worth noting that surface tension of a mixture, as expected, tends to change with concentration. The decrease in surface tension when increasing ethanol concentration is however not linear. The gradients in surface tension induced by concentration variations could be readily traced following the trend in Figure 3.

## 2.2. Flow structure evolution

In order to represent the flow intensity across the base section of the drop, Figure 4, a space-averaged vorticity is adopted, it is hereafter referred to as average vorticity,  $\bar{\omega}_z(t)$ . The results of spatio-temporal velocity, Figure 5, as well as average vorticity, Figure 6, show consistently, and for the three studied concentrations, three distinct stages in flow structure. During the first stage, multiple vortices are observed, the number of these latter reduces as evaporation proceeds. The intensity of average vorticity is found to be roughly constant during this stage albeit with some fluctuations. The onset of the first stage can be clearly seen as a sharp increase in average vorticity after the drop is deposited. This is

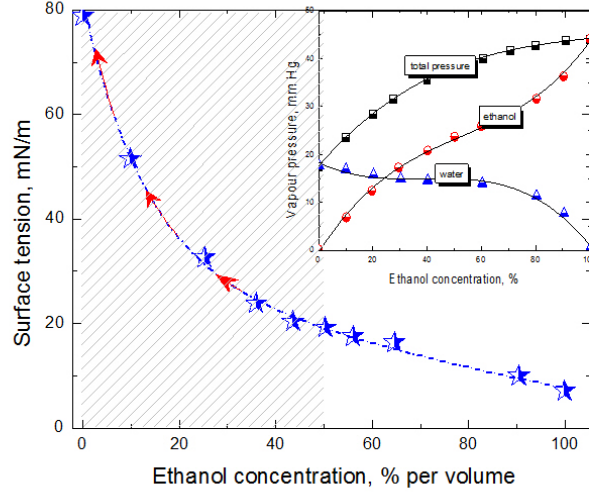


FIGURE 3. Surface tension of the binary mixture, the range of concentrations is highlighted. Inset shows partial vapour pressure for water-ethanol mixture.

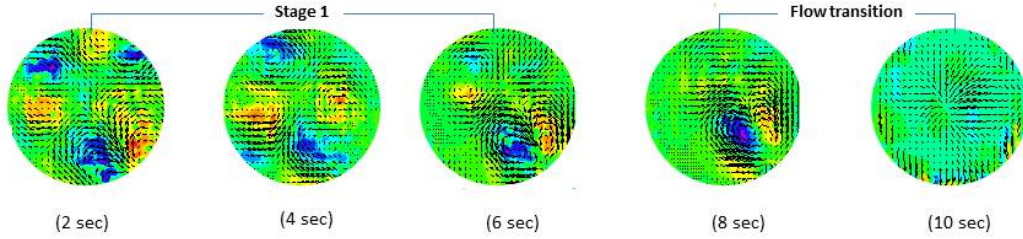


FIGURE 4. Flow structure evolution throughout the three distinct stages of evaporation for 50 % initial concentration. Velocity vectors and vorticity are superimposed, clockwise vorticity is represented in blue and counter-clockwise in red.

more noticeable in the case of 25% and 50% concentrations though, Figure 6. This first stage of constant average vorticity is followed by a decay in average vorticity intensity and finally an outward flow where vorticity is virtually nil which is reminiscent of evaporating pure water drops. The transition stage is characterised by a decay in average vorticity but also by a spike in radial velocity before settling in the last outward flow stage, Figure 5 and Figure 6. We can only speculate about the spike in velocity during transition, it is believed however that gradients along the interface intensify during the stage where the last bits of ethanol evaporate from the surface. Which might be due to some areas of the surface being significantly depleted in ethanol.

The intensity of the average vorticity,  $\bar{\omega}_z(t)$  during the first stage is found to depend on the initial concentration. The lifetime of the drop as well as the extent of the successive stages are also dependent on the initial concentration. We can however, for the purpose of the analysis to follow, overcome this variability by normalising the average vorticity by the initial value,  $\tilde{\omega} = \frac{\langle \omega \rangle}{\langle \omega_0 \rangle}$ , and initialising the time by the transition time,  $t^* = t - t_0$ , as will be presented further. In so doing, one can compare the trends for various initial concentrations.

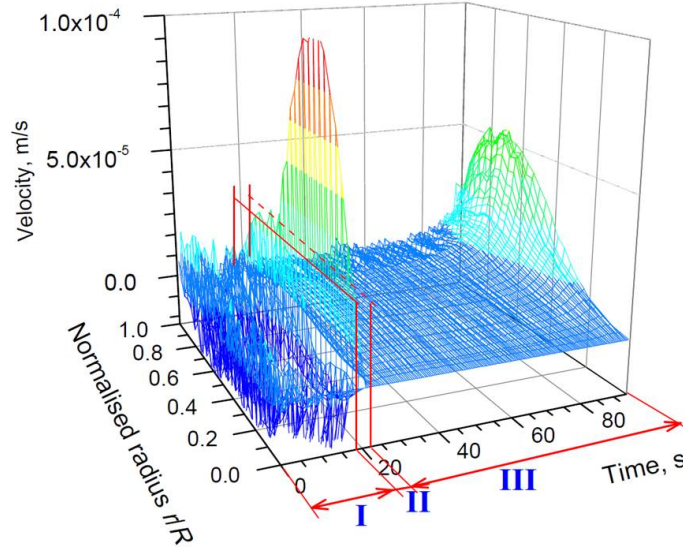


FIGURE 5. A sample of spatio-temporal evolution of the measured radial velocity for a 5 % ethanol binary evaporating drop. The three stages are highlighted, (I) multiple vortices, (II) transition and (III) outward flow.

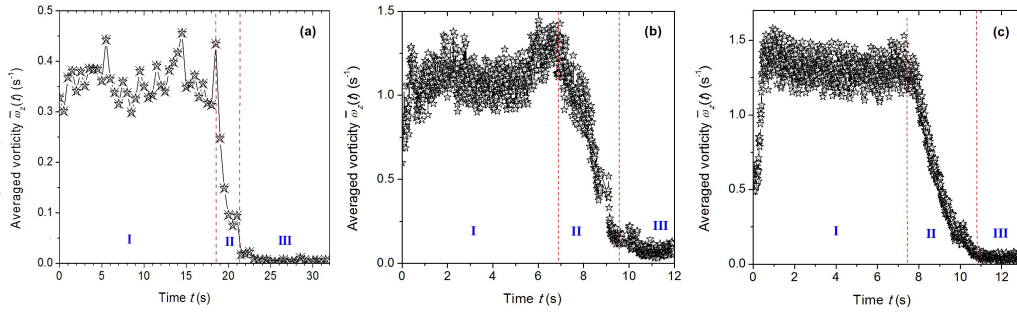


FIGURE 6. Evolution of averaged vorticity,  $\bar{\omega}_z(t)$  in time for binary evaporating drops at initial ethanol concentrations of (a) 5 %, (b) 25 % and (c) 50 % per volume. Stages of evaporation are indicated.

### 3. Analysis

In the following sections, the successive stages of evaporation and flow structure evolution within evaporating binary drops as revealed by the experimental data presented above are analysed. Each stage is discussed with a focus on the physical mechanisms as well as interpretation of the observations.

#### 3.1. First stage of evaporation, multiple vortices

In order to understand the nature of the observed flow we proceed by considering potential physical mechanisms responsible for the observed flow. Convection in a system such as the one under investigation *i.e.* volatile small drops, can be either gravity or surface tension (Marangoni) driven. The conditions for the onset of Buoyancy, thermal or solutal Marangoni convection are determined by relevant dimensionless numbers.



These are *Rayleigh*,  $Ra = \frac{\Delta C \frac{\partial \gamma}{\partial C} L^3 g}{D \nu}$  and thermal or solutal *Marangoni* number,  $Ma_s = \frac{(\frac{\partial \gamma}{\partial C}) \times \Delta C \times L}{\mu \times D_l}$ , respectively. In order for the flow to ensue, a threshold represented by critical numbers must be surpassed. Ethanol being lighter than water and more volatile will tend to concentrate near the interface. Having the lightest component on top will lead to a stable configuration, as far as Rayleigh driven convection is concerned. We have also estimated the *Bo*, *Bond*,  $Bo = \frac{\rho L^2 g}{\gamma}$  number, as defined above, it was found to be of the order of 0.1. This implies that drops will not be deformed by gravity and will adopt a spherical shape. The convection revealed by the experiments in the present study is unlikely to be buoyancy driven since the sizes of the drops were very small *i.e.* below the capillary length. In addition, the comparison between mixture drops and pure ones, allowed to rule out buoyancy driven flows. Indeed if gravity was driving vortices during the first stage of evaporation, this should also be noticeable for the pure drops. The fact that no vortices were observed for pure water and pure ethanol cases indicates that gravity can indeed be ruled out. We therefore concluded that buoyancy cannot be the mechanism behind observed multi-vortices convection. The two remaining mechanisms for convection are surface tension driven flows either thermocapillary or solutal in nature. In order to assess any contribution of thermocapillarity to the observed flow, we used infrared thermography as a non-intrusive technique to map the liquid interface temperature. The collected data showed small but measurable variations. We estimated the thermal *Marangoni* dimensionless number based on recorded temperature differences and we found this to be sub-critical in all cases. Therefore, we concluded that the observed flow convection to be more likely of solutal *Marangoni* in nature. An additional flow mechanism is related to continuity, Deegan *et al.* (1997). This flow is due to higher evaporation near the contact line. It is believed to be present for both binary and pure drops and in all stages of evaporation.

Based on the experimental observations, we can propose a scenario for the development of concentration gradients leading to convection vortices. Whilst at  $t = 0$ , the concentration is uniform, subsequently and because of selective evaporation, ethanol is quickly depleted at the interface as it preferentially evaporates. Furthermore, evaporation is not uniform along the interface, being highest near the contact line. This creates a concentration gradient between the bulk and the interface, which drives a diffusion flux. In the case of volatile binary drops, the amount of ethanol is limited and depends essentially on the initial concentration. Because of the limited 'reservoir' of ethanol, this tends to be depleted as evaporation progresses. As a result, both concentrations in the bulk and on the interface tend to reduce in time. Concentration gradients between the bulk and the interface are good indicators of the gradients along the interface. Indeed, any gradient developing on the interface will be at best of the same magnitude as the difference between the bulk and the interface. Figure 11 (Appendix 1) gives a qualitative understanding of the evolution of various concentrations and gradients for the diffusive case. The presence of convection during the first stage however, is likely to induce mixing and would tend to smooth concentration gradients.

In what follows we attempt a quantitative analysis of the experimental data, including evaporation rates and profile measurements. Starting from evaporation rates evolution presented in Figure 2, we calculate the flow velocity driven by continuity within the drop. This velocity is then used to estimate the Reynolds number,  $Re = \frac{\rho \times V_{continuity} \times L}{\mu}$ , which will be representative of the magnitude of the flow driven by continuity. **We then use the same data of evaporation rates to find the evolution of ethanol concentration**

within the drop in time. The only assumption made at this stage is that the volume evaporated during the first stage is mainly ethanol, because of preferential evaporation. Based on the evolution of ethanol concentration in time we can then calculate the solutal Marangoni number using the maximum possible concentration difference which can exist along the interface. This is based on the idea that at any given time, the maximum possible (upper limit) concentration difference along the interface corresponds to the situation where at one point the concentration of ethanol is that in the bulk and on another point it would be that of pure water because of evaporation (of ethanol). In essence, for all the analysis we use the evaporation rates measured from drop shape analysis to deduce the evolution of concentration gradients. Indeed as evaporation is not uniform along the interface, being highest near the contact line, some areas of the interface will be depleted in ethanol whilst other will have the same ethanol content as the bulk. This is the most extreme case where a maximum concentration difference is envisaged. This allows us to estimate the maximum possible concentration gradient along the interface as,  $\Delta C_{Max} = C_{Max} - 0$ . The flow velocity in the liquid adjacent to the interface, along which the gradient exists, and which ensues as a result of solutal capillary stress is given by  $V_{Ma} \sim Ma$ . The velocity due to gradients in concentration is proportional to the Marangoni number estimated using concentration gradients along the interface. For the sake of simplicity of the analysis which follows, we assume the exponent to be unity. We can thus compare the ratio between the two velocities within the drop. The ratio between Marangoni driven flow to continuity driven flow, *i.e.*  $\frac{V_{Ma}}{V_{Re}}$  which is equivalent to taking the ratio,  $\frac{Ma}{Re}$ . The ratio between these two dimensionless numbers will express the magnitude of the flow driven by solutal Marangoni effect compared to the one driven by continuity. The ratio should be a good indicator of which of the two effects is dominant and hence can clearly describe transition from one stage of evaporation to another. The flow structure during stage II is a transition where Marangoni driven flow is weakening and continuity driven flow is taking over. The velocity of flow during stage I, is related to the magnitude of solutal Marangoni number. Whereas the velocity in stage III can be described by a *Reynolds* number based on the velocity of outward flow. In order to compare these two flows, we can take the ratio between the two dimensionless numbers representing each, *i.e.* *Marangoni* number and *Reynolds* number,  $\frac{Ma_s}{Re} \sim \frac{V_{Marangoni}}{V_{continuity}}$ . The solutal Marangoni number is defined as,  $Ma_s = \frac{(\frac{\partial \gamma}{\partial C}) \times \Delta C \times L}{\mu \times D_l}$ . The Reynolds number is defined as,  $Re = \frac{\rho \times V_{continuity} \times L}{\mu}$ . The ratio between *Marangoni* and *Reynolds* numbers yields a new number  $\frac{Ma_s}{Re} = \frac{(\frac{\partial \gamma}{\partial C}) \times \Delta C}{\rho \times V_{continuity} \times D_l}$ . This new ratio is relevant to all situation where there are solutal Marangoni driven flows adjacent to an interface with a drift current in the underlying liquid. Indeed any configuration where solutal *Marangoni* flow driven by gradients along the interface is simultaneously taking place with an underlying flow in the bulk of the liquid, the new dimensionless number will be of relevance.

A graph showing the evolution of the ratio,  $\frac{Ma_s}{Re}$  is presented in Figure 7 and in dimensional form in Figure 8(b). The results presented in Figure 7 are calculated according to the procedure explained in the previous section. **That is, using the data about evaporation rates and droplets profile, given in Figure 2, the flow velocity due to continuity is deduced since the flow has to compensate exactly for the evaporated mass. We estimated this velocity half-way between the centre of the drop and the contact line, *i.e.* at  $r = R/2$ . This velocity due to mass conservation is used to calculate the *Reynolds* number. Furthermore, the veloc-**

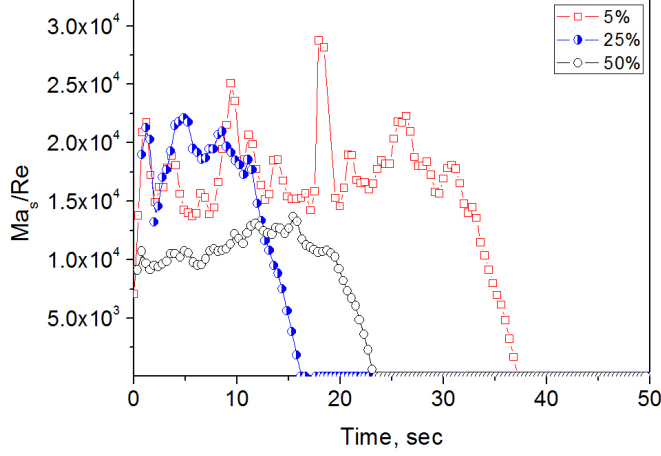


FIGURE 7. Evolution of the ratio  $\frac{Ma_s}{Re}$  which reflects the three successive stages identified with PIV.

ity of the flow calculated using evaporation rate data, Figure 2, is compared to direct measurements of the flow obtained using PIV as described in, Hamamoto *et al.* (2011) and Christy *et al.* (2011). The agreement between these two velocities is very satisfactory. The order of magnitude of velocities calculated from the evaporation rate and using continuity are of the order  $10^{-5}$ ,  $m/s$ , which are of the same order as the experimental PIV measurements. When normalised with the initial values, the ratio  $Ma_s/Re$  clearly reflects the evolution of normalised and initialised vorticities evolution in time as shown in Figures 8(a) and (b).

### 3.2. Second stage of evaporation, viscous dissipation and flow transition

In the following section, we set about analysing the second stage of evaporation and flow structure. This stage is characterised by a transition in flow structure, from multiple vortices to an outward flow. The transition is sudden and a rapid decline of the magnitude of vorticity is observed.

Since transition in flow occurs at the end of stage I, which corresponds to the depletion of ethanol content, diffusion of this latter in water is examined. Diffusion of ethanol in water is obviously a crucial step in sustaining concentration gradients on the interface which might explain flow transition. The diffusion coefficient of ethanol in water is of the order of  $1.5 \cdot 10^{-9} m^2/s$ . Assuming a diffusion length-scale of the order of the radius of the drop *i.e.*  $10^{-3}m$ , one gets a time of the order of 1000 *seconds*. This clearly is three orders of magnitude larger than the transition time which is of the order of seconds. Hence, diffusion of ethanol alone cannot be a satisfactory explanation for the observed transition in flow. An alternative physical mechanism to be considered in explaining the observed flow transition is viscous dissipation. Indeed, once the driving force for solutal *Marangoni* flow switches off, the flow has to decay under the resistance of viscosity. This mechanism will be examined in the following section.

The evolution of the flow (represented by average vorticity) with the initial condition, at  $t = 0$ ,  $\omega = \omega_0$  and subsequently dampened by viscous dissipation is examined. The evolution of such a vortex within the droplet is governed by the incompressible Navier-Stokes conservation equation when expressed by vorticity,  $\omega = \vec{\nabla} \times \vec{V}$  is given by,

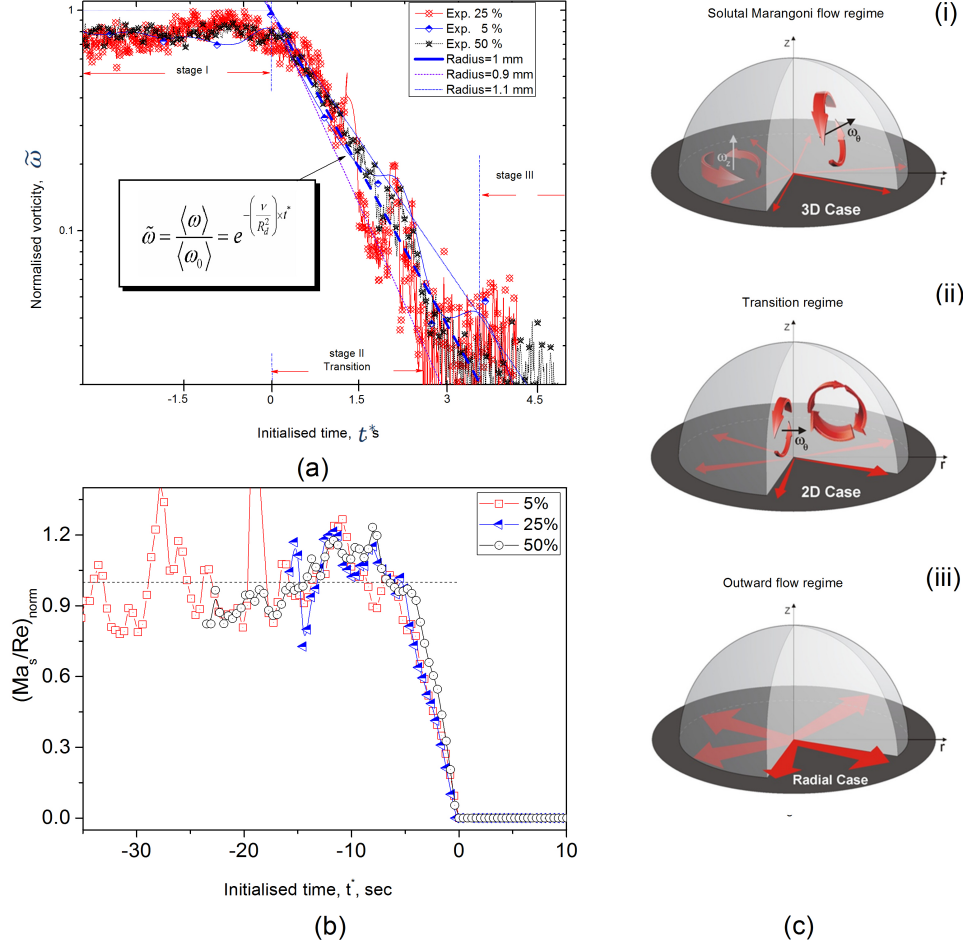


FIGURE 8. Stages of the flow, (a) Normalised experimental vorticity, (b) Ratio of solutal Marangoni number and Reynolds number evolution and (c) Illustration of the flow stages

$$\frac{\partial \omega}{\partial t} + V \cdot \nabla \omega = \omega \cdot \nabla V + \nu \nabla^2 \omega \quad (3.1)$$

The approximate solution for viscous dissipation is given by (see Appendix 2 for further details),

$$\langle \omega \rangle \sim \langle \omega_0 \rangle e^{-\frac{\nu \times t^*}{R_d^2}} \quad (3.2)$$

Where  $\langle \omega \rangle$  is the space averaged vorticity. For considered experimental cases, drop sizes are of the order of  $R_d \approx 10^{-3}m$  and the kinematic viscosity is taken as that of water hence of the order  $\nu \approx 10^{-6}m^2/s$ . The value of viscosity is assumed as that of water since transition occurs at the end of the first stage, so most of ethanol would have completely evaporated. Using these values for radius and viscosity, one gets, for a millimeter drop base radius,  $\frac{\nu}{R_d^2} \approx 1$ . This is the case for 25 % concentration. From equation (3.2), and considering our experiments, it can be noted that the exponential decay constant

slightly changes with drop base radius, it ranges from 0.83 to 1.23 for 5 % to 50 % initial concentration. However, it is expected that for same size drops, the evolution of vorticity during transition stage to be the same. It is noteworthy that the hypothesis of a viscous dampening of the flow leads to an order of magnitude for the duration of transition very comparable to the one revealed by experiments, see Figure 6. Furthermore, when normalised with the initial value, the transition in flow is found to be the same regardless of the initial concentration, Figure 8 (a).

### 3.3. Last stage of evaporation, outward flow

The last stage of evaporation is characterised by an outward flow which accelerates in time. The outward flow is the result of continuity driven by evaporation at the contact line. This flow due to mass conservation was first reported by Deegan *et al.* (1997). It was found responsible for the "coffee" ring stain formation observed whenever suspension drops evaporate. The outward flow during the last stage of evaporation exhibits an increasing flow velocity, Marin *et al.* (2011). The increase in flow velocity can be an order of magnitude greater compared at the start of the evaporation. This is due to thinning of the drop and the reduction of area available for flow which has to compensate for evaporation, Hamamoto *et al.* (2011), see Figure 9. Indeed the evaporation rate at the contact line of pinned drops is constant, because of the thinning of the drop and reduction of cross sectional area, the flow has to accelerate to compensate for evaporation. In Figure 10 the spatio-temporal flow field during the evaporation of a pure water drop is compared with that of a 5 % ethanol drop during its last stage of evaporation. The comparison clearly shows that the two spatio-temporal profiles are similar qualitatively and quantitatively. The order of magnitude of radial velocities is very comparable as well

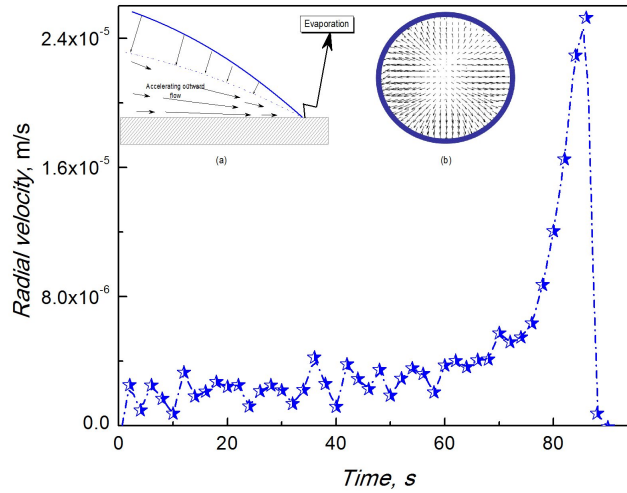


FIGURE 9. Measured radial velocity in time at  $0.1R$  from contact line. Inset: (a) Sketch of outward flow driven by continuity, (b) PIV data for outward flow. This is observed during the last stage of evaporation of binary drops and pure water ones, see Hamamoto *et al.* (2011) and Marin *et al.* (2011). Inset shows (a) a sketch for the outward flow driven by evaporation and (b) PIV velocity arrows

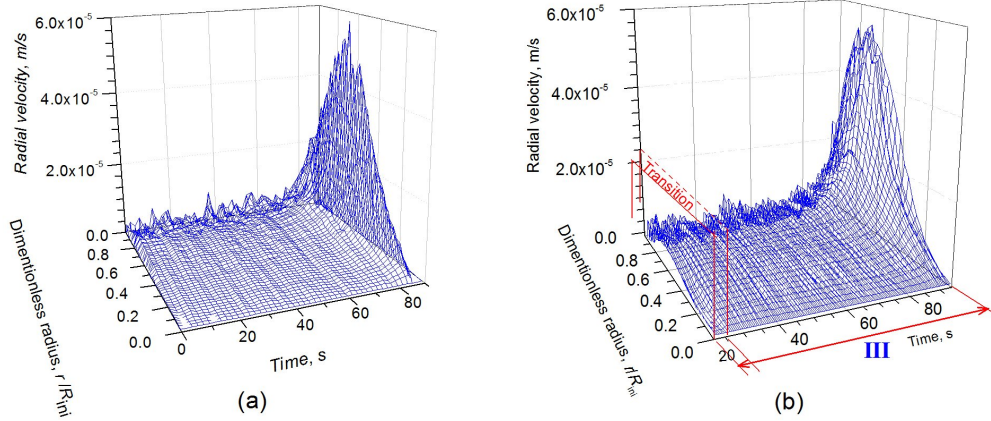


FIGURE 10. Spatio-temporal flow profile for (a) pure water drop, (b) the last stage of evaporation of a 5% ethanol drop.

as the radial profile and time evolution. Worth noting that these orders of magnitude of flow velocities are very comparable to the ones calculated using evaporation rate from Figure 2, as discussed previously.

#### 4. Discussion and conclusions

The study of evaporation and internal flow field in binary drops revealed three distinct stages of evaporation and flow structure. Because of selective evaporation, ethanol (the more volatile component) diffuses from the bulk to the interface where it evaporates. The non-uniform evaporation and the fact it is localised near the three phase contact line is well established, Deegan *et al.* (1997). This non-uniformity in evaporation induces concentration gradients along the interface. Such gradients induce surface tension gradients, which are the driving force for flow motion expressed as  $\frac{\partial u_\theta}{\partial n} \simeq -Ma_s \times \frac{\partial C_i}{\partial \tau}$ , here the solutal *Marangoni* number is given by,  $Ma_s \simeq -\frac{\partial \sigma}{\partial n} \Delta C \frac{R_d}{\mu D_l}$ . The non-uniform distribution of evaporation along the interface leads to local concentration gradients. These latter generate surface tension gradients and lead to solutal *Marangoni* flow. By the end of the first stage, most (if not all) ethanol would have evaporated. Concentration gradients are therefore too weak to sustain the flow *i.e.* solutal *Marangoni* number becoming sub-critical. Once the driving force for the flow switches off, the flow evolution of the flow is dictated by viscous forces. The decay in vortices intensity is entirely controlled by viscous dissipation. This transition stage exhibits an exponential evolution in time, starting from the initial vorticity and finishing when this vanishes. The last stage is reminiscent of the pure water case where an outward flow is observed. The monotonous outward flow during the last stage is shown to result from continuity, Hamamoto *et al.* (2011). This is due to the fact that evaporation takes place exclusively near the three phase contact line, consequently the flow in the drop is driven to compensate for mass loss by evaporation. The observation that regardless of the initial concentration, the transition in flow is virtually the same is a strong support of this analysis. Indeed, the experimental data span over a wide range of concentrations. Despite this, the transition in flow is found to occur in the same fashion.

The transition between the first stage where the flow structure is dominated by vigorous multiple vortices to an outward flow, indicates that stage I, is dominated by *Marangoni* flow driven by concentration gradients on the interface. The flow during this stage is

inherently three-dimensional (3D) and asymmetrical, whereas the flow structure in stage III is more one-dimensional (1D) and symmetrical, Figure 8 (c). During the first stage of evaporation, concentration gradients at the interface are large enough to induce the vigorous observed flow structure. In comparison the flow driven by mass conservation (continuity) is rather negligible during this first phase of evaporation. As evaporation proceeds, concentration gradients and hence solutal *Marangoni* number weakens then continuity driven flow starts to take over. Following the flow transition and during stage III, the outward flow driven by mass conservation (continuity) becomes dominant and the solutal Marangoni flow is negligible. This evolution of flow structure and the distinct stages are found to be well described by the ratio of the two dimensionless numbers,  $Ma_s/Re$ .

A simple analysis yielded expression (3.2) which describes the evolution of vorticity in time, initially at  $\omega_0$  and then decaying under the resistance of viscosity. This expression in its normalised form is independent of initial concentration, the dimensional vorticity however does depend on the initial concentration through the initial vorticity  $\omega_0$ . The relation between the initial vorticity and initial concentration is beyond the scope of the present analysis which aims primarily to address the question of the mechanism behind the transition in flow. The average vorticities from Figure 6 are normalised by the initial vorticity (from the first stage) and time is initialised by transition time. The normalised vorticities are then plotted for the three initial concentrations on the same graph in Figure 8 (a). The plot in Figure 8 (a) shows that data for different initial concentrations collapse to a single curve (for similar size drops) which reveals the distinct three stages in flow structure. The expression for dimensionless vorticity obtained in equation (3.2) is then superimposed on the experimental data for all concentrations. The agreement is more than satisfactory because of the simple analytical exponential decay in vorticity. The slope of the transition decay is affected by the drop size, Figure 8 (a). Considering that no fitting parameters or adjustment factors are used in the comparison, the achieved agreement is a strong support for the hypothesis of a viscous dissipation mechanism which controls transition of the flow. Finally, the observation that during the first stage of evaporation, the number of vortices reduces as evaporation progresses is an interesting trend. The fact that concentration gradients, which are the driving force for the flow are also decreasing during the first stage, raises the question about the correlation between the two *i.e.* number of vortices and concentration gradients. We can only speculate at this point about the analogy between these observations and turbulence *vs* energy dissipation. This remains however an open question revealed by this study worth the attention of researchers in the field. Nonetheless, and despite outstanding questions the presented study stands as pioneering in the investigation of internal flow in volatile mixture drops. The implications of the internal flow and its behaviour is crucial in understanding energy transport mechanisms in these systems. The obtained results illustrate that, besides the complex transient and multiple cells observed flow, solutal gradients are the origin of the flow and reveal the existence of a threshold below which the flow driving force became too weak to sustain flow.

## REFERENCES

- CHENG, A. K. H., SOOLAMAN, D. M. & YU, H. 2006 Evaporation of micro droplets of ethanol-water mixtures on gold surfaces modified with self-assembled monolayers. *J. Phys. Chem. B* **110**, 11267–11271.

- CHRISTY, J., HAMAMOTO, Y. & SEFIANE, K. 2011 Flow transition within an evaporating binary mixture sessile drop. *Phys. Rev. Lett.* **106**, 205701.
- DEEGAN, R. D., BAKAJIN, O., DUPONT, T. F., HUBER, G., NAGEL, S. R. & WITTEN, T. A. 1997 Capillary flow as the cause of ring stains from dried liquid drops. *Nature* **389**, 827–829.
- ERBIL, H.Y. 2012 Evaporation of pure liquid sessile and spherical suspended drops: A review. *Advances in Colloid and Interface Science* **170**, 6786.
- GHASEMI, H. & WARD, C. A. 2010 Energy transport by thermocapillary convection during sessile-water-droplet evaporation. *Phys. Rev. Lett.* **136**102 **13**.
- HAMAMOTO, Y., CHRISTY, J.R.E. & SEFIANE, K. 2011 Order-of-magnitude increase in flow velocity driven by mass conservation during the evaporation of sessile drops. *Phys. Rev. E* **05**1602 **83**.
- HOPKINS, R.J. & REID, J. P. 2006 A comparative study of the mass and heat transfer dynamics of evaporating ethanol/water, methanol/water, and 1-propanol/water aerosol droplets. *J. Phys. Chem. B* **110**, 3239–3249.
- HU, H. & LARSON, R. G. 2006 Marangoni effect reverses coffee-ring depositions. *J. Phys. Chem. B* **110**, 7090–7094.
- MARIN, A.G., GELDERBLOM, H., LOHSE, D. & SNOEIJER, J. H. 2011 Rush-hour in evaporating coffee drops. *Phys. Fluids* **23**, 3239–091111.
- RISTENPART, W. D., KIM, P. G., DOMINGUES, C., WAN, J. & STONE, H. A. 2007 Influence of substrate conductivity on circulation reversal in evaporating drops. *Phys. Rev. Lett.* **234**502 **99**.
- ROWAN, S. M., NEWTON, M. I., DRIEWER, F. W. & MCHALE, G. J. 2000 Evaporation of microdroplets of azeotropic liquids. *J. Phys. Chem. B* **104**, 8217–8220.
- SEFIANE, K. & BENNACER, R. 2011 An expression for droplet evaporation incorporating thermal effects. *J. Fluid Mech.* **667**, 260–271.
- SEFIANE, K., DAVID, S. & SHANAHAN, M. E. R. 2008 Wetting and evaporation of binary mixture drops. *J. Phys. Chem. B* **112**, 11317–11323.
- SEFIANE, K., WILSON, S. K., DAVID, S., DUNN, G. & DUFFY, B. R. 2009 On the effect of the atmosphere on the evaporation of sessile droplets of water. *Phys. Fluids* **21**, 062101.
- YOUNG, T. 1805 An essay on the cohesion of fluids. *Phil. Trans. R. Soc. Lond.* **95**, 65–87.



## 5. Appendix 1

In addition to the above analysis, diffusion can be solved within the drop to deduce concentrations and their evolution with time. In the case of the evaporation of binary drops the more volatile component evaporates first because of selective evaporation. This component diffuses from the bulk of the drop to the interface to evaporate. The evaporated component then diffuses in the gas phase which is a mixture of air and vapour. The diffusion equation on liquid domain can be written as follows,

$$\frac{\partial C}{\partial t} = D_l \times \nabla^2 C \quad (5.1)$$

Where  $D_l$  is the diffusion coefficient of ethanol in water (in liquid phase).

With the following boundary conditions; at  $t = 0$ ,  $C(r, \theta, 0) = C_0$  and at substrate interface,  $z = 0$ ,  $\frac{\partial C}{\partial z} \big|_{z=0} = 0$ .

At  $t > 0$  and on interface  $R = s(\theta)$ ,

$$\frac{\partial C}{\partial n} \big|_{int} = h(C_{int} - C_\infty) \quad (5.2)$$

Where  $h$  is the modified diffusion-convection coefficient on the liq-air interface including the modifying coefficient from gas to liquid ethanol concentration. Using the following characteristic length,  $L_{ref} = R_d$ ,  $\Delta C = C_0 - C_\infty$  ( $C_\infty$  is equal to zero in the present study as no ethanol is contained in the air) and  $\tau_{ref} = \frac{R_d^2}{D_l}$  so the equation becomes:

$$\frac{\partial C^*}{\partial Fi} = \nabla^{*2} C \quad (5.3)$$

and

$$\frac{\partial C^*}{\partial n^*} \big|_{int} = Bi_s C_{int}^* \quad (5.4)$$

This linear problem has an analytical solution using separation of variables (or Laplace transformation, Green function). The solutal Biot and Fick numbers are,

$Bi_s = \frac{hR_d}{D_l}$ ,  $Fi = \frac{D_l \times t}{R_d^2}$ , respectively.

$$C^*(r, t) = \frac{(C(r, t) - C_\infty)}{(C_0 - C_\infty)} = \frac{2}{\frac{r}{R_d}} \sum_{n=1}^{\infty} \left( e^{(-Fi)} \right) \times \frac{\sin(\lambda_n) - \lambda_n \cos(\lambda_n)}{\lambda_n^2 [\lambda_n - \sin(\lambda_n) \cos(\lambda_n)]} \times \sin\left(\lambda_n \frac{r}{R_d}\right) \quad (5.5)$$

Where the eigenvalues  $\lambda_n$  are the solutions of the equation  $\lambda \cot(\lambda) = (1 - Bi_s)$

The surface concentration are obtained for  $r = R_d$  and the center (bulk) is deduced for  $r \rightarrow 0$  and given by,

$$C^*(0, t) = \frac{C(0, t) - C_\infty}{(C_0 - C_\infty)} = 2 \sum_{n=1}^{\infty} \left( e^{(-Fi)} \right) \times \frac{\sin(\lambda_n) - \lambda_n \cos(\lambda_n)}{\lambda_n - \sin(\lambda_n) \cos(\lambda_n)} \quad (5.6)$$

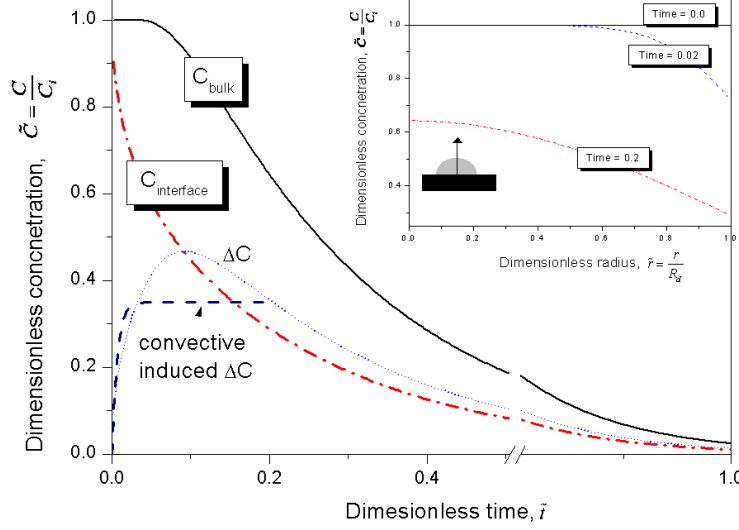


FIGURE 11. Dimensionless concentrations and gradient evolution in a diffusive mode.

## 6. Appendix 2

In what follows, we propose a scale analysis description of the flow time evolution (represented by average vorticity) with the initial condition, at  $t = 0$ ,  $\omega = \omega_0$  and subsequently damped by viscous dissipation. The flow of such a vortex within the droplet is governed by the incompressible Navier-Stokes conservation equation when expressed by vorticity,  $\omega = \vec{\nabla} \times \vec{V}$  is given by,

$$\frac{\partial \omega}{\partial t} = \nu \nabla^2 \omega + \overbrace{\omega \cdot \vec{\nabla} V - V \cdot \vec{\nabla} \omega}^{\text{inducing vortex deformation}} + \overbrace{S}^{\text{barocline production}} \quad (6.1)$$

In order to capture the scale order, we use the assumption of weak vortex deformation or equivalent order *i.e.*  $V \cdot \vec{\nabla} \omega \approx \omega \cdot \vec{\nabla} V$  (or 2D main flow, with axial symmetry) and negligible source term  $S$  ( $\nabla p \cdot \nabla \rho \approx 0$  and  $\nabla \sigma \approx 0$ ) so we obtain,

$$\frac{\partial \omega}{\partial t} \approx \nu \nabla^2 \omega \quad (6.2)$$

Based on previous space and time reference scales (Appendix 1) we get,

$$\frac{\partial \omega}{\partial F_v} \approx \nabla^2 \omega \quad (6.3)$$

Where  $F_v = \frac{\nu \times t^*}{R_d^2}$ . Expressed on the given volume area  $\Omega$ ,

$$\int_{\Omega} \frac{\partial \omega}{\partial F_v} d\Omega \approx \int_{\Omega} \nabla^2 \omega d\Omega \quad (6.4)$$

based on classical Reynolds transport theorem (neglecting  $((V \vec{n}) \cdot \omega)$ ) and Green-Ostrogradski

theorem it becomes,

$$\Omega \frac{\partial \langle \omega \rangle}{\partial F_v} \approx \int_{\Sigma} \nabla \omega \cdot \vec{n} \, d\Sigma \quad (6.5)$$

Where  $\langle \omega \rangle$  is the space averaged vorticity. The surface, normal vector  $\vec{n}$  and interface are related to the droplet radius. Due to the free surface condition, the main vorticity gradient is on the droplet base (substrate/liquid interface)  $\int_{\Sigma} \nabla \omega \cdot \vec{n} \, d\Sigma \approx \int_{\bar{r}=0}^1 \nabla \omega|_{z=0} \cdot 2\pi \bar{r} \, d\bar{r}$ . We will keep only the main order of the damping effect using the non slip boundary condition on the substrate  $\nabla \omega|_{z=0} \sim \frac{-\omega}{1} \dagger$ .

Based on the vorticity damping tendency we can obtain,

$$\frac{\partial \langle \omega \rangle}{\partial F_v} \sim -\langle \omega \rangle; \int_{\langle \omega_0 \rangle}^{\langle \omega \rangle} \frac{\partial \langle \omega \rangle}{\langle \omega \rangle} \sim \int_0^{F_v} -\partial F_v \quad (6.6)$$

The solution is an exponential decay one, illustrating the vorticity damping due to viscous effects,  $\frac{\langle \omega \rangle}{\langle \omega_0 \rangle} \sim e^{-F_v}$ , or,

$$\langle \omega \rangle \sim \langle \omega_0 \rangle e^{-\frac{\nu \times t^*}{R_d^2}} \quad (6.7)$$

The authors would like to acknowledge the contribution of Y. Hamamoto and J. Christy to the experimental part of this study as well as O. Rahli for assistance in producing illustration in Figure 7.

$\dagger$  the dimensionless spatial variable  $\bar{r} \in \llbracket 0; 1 \rrbracket$